

Successive earthquake-tsunami analysis to develop collapse fragilities¹

Sangki Park², John W. van de Lindt³, Daniel Cox⁴, Rakesh Gupta⁵, and
Francisco Aguiniga⁶

Abstract

Over the last half-century, scientists and engineers have developed methods to better understand and mitigate the damage caused by tsunamis. According to U.S. Federal Emergency Management Agency (FEMA) P646, buildings in many regions including the U.S. Pacific Northwest, will experience substantial ground shaking from an offshore earthquake that precedes a tsunami and then experience the tsunami forces themselves. Thus, both hazards should be considered in computing the damage and collapse risk to buildings. This paper summarizes a basic approach to numerically consider the successive seismic and tsunami risk to buildings in near-field tsunami regions such as the U.S. Pacific Northwest.

Key Words: Fragility curve; hysteresis model; tsunami; earthquake; collapse

Introduction

¹ Submitted to the *Journal of Earthquake Engineering*, June 2011; Revised version submitted Dec 2011.

² Ph.D. Candidate, Department of Civil and Environmental Engineering, Colorado State University

³ [Contact Author] Professor and Drummond Chair, Department of Civil, Construction, and Environmental Engineering, University of Alabama; Box 870205, Tuscaloosa, Alabama, 35487-0205, USA, 1-205-348-2209; jwvandelindt@eng.ua.edu

⁴ Professor, School of Civil and Construction Engineering, Oregon State University, Corvallis, OR 97331, USA

⁵ Professor, Department of Wood Science and Engineering, Oregon State University

⁶ Assistant Professor, Department of Civil Engineering, Texas A&M University, Kingsville, TX 78363, USA

Tsunamis are among the most destructive of natural hazard forces mainly because of their intensity and the breadth of their impact on human lives. The 2004 Indian Ocean tsunami, triggered by a 9.2 magnitude undersea earthquake, killed over 200,000 people in 11 countries. Coastal communities were inundated with waves up to 30 meters (100 feet) high and entire coastal regions devastated. This tsunami has been characterized as one of the worst natural disasters in human history. The 2010 Chile earthquake, which was also offshore, generated a tsunami that killed several hundred people. Figure 1 shows the town of Talcahuano in Chile following the tsunami with a wave recorded of 2.5 meters (8.2 feet). Figure 1 shows the devastation that can be caused by a moderate tsunami, underscoring the need to better understand wave/structure interaction. The 2011 Great Tohoku Japan earthquake resulted in a devastating 10m (33 feet) wall of water that killed more than 15,000 people in Northeastern, Japan. Every year there are approximately 20 tsunami-generating earthquake events and five of these are large enough to generate tsunamis capable of causing economic damage and result in the loss of human life.

It is well understood that earthquake ground shaking reaches a structure before a tsunami generated by that earthquake simply because of the shear wave velocity in soil and rock versus the wave velocity in water. FEMA P646 (2008) recommends the consideration of both the earthquake demand from shaking and the tsunami demand for the design of structures in certain coastal regions such as the U.S. Pacific Northwest. While this may not be current practice in most areas, it is important to develop a better understanding of how one hazard affects the other since they may occur rapidly in succession, i.e. without the ability to repair between the loadings. Building design codes are based on load occurrence probability and resistance statistics of the

components making up a building system, but tsunamis are typically not considered in design except in very rare circumstances.

This paper presents the results of a numerical study to examine the effect of earthquake motion on tsunami collapse fragilities and present a basic technique for applying these successive hazards to a numerical model. Initially, the methodology to develop a structural collapse fragility for tsunami loading is presented. Then, prior to computing the collapse fragility from tsunami loading, a nonlinear time history analysis for the earthquake that may have produced the tsunami is performed. Damage is allowed to accumulate in the model so the successive effect of earthquake loading and tsunami loading can be quantified in terms of collapse fragilities. Figure 2 provides a schematic overview of the two-stage analysis procedure used in this study and the general shape of a fragility from this two-stage analysis. The tsunami loading characterized by FEMA P646 (2008) was used in the second stage of the analysis. In order to do this, a program was developed and termed the Sequential Seismic and Tsunami Analysis Program (SSTAP).

Hysteresis models have been used extensively for steel, concrete, and wood structures and their subassemblies for many years in earthquake engineering. A hysteresis model defines the shape of the force-deformation loops with a set of empirical rules to allow one to perform nonlinear time history analysis. Figure 3 shows an example of a typical 10-parameter hysteresis model that has been used to model wood shear walls and wood buildings over the last decade and will be used in the stage one portion of the analysis for the illustrative example in this study. The CUREE hysteresis model shown in Figure 3 is a single-degree-of-freedom (SDOF) hysteretic model that provides the resisting force for wood shearwalls under cyclic loading by using an exponential

backbone curve and piecewise linear loading and unloading paths (Folz and Filiatrault 2001, 2004a, b). More sophisticated hysteresis models are also available to use (e.g. Pei and van de Lindt 2008; Collins 2009; Xu and Dolan 2009a, b).

The design of coastal structures in a tsunami-hazard zone should take into account loading from tsunamis but the occurrence rates are still not well understood. In the present study the issues of occurrence rate, i.e. tsunami hazard level, are not addressed. Rather, it is assumed that the tsunami occurs and the collapse probabilities computed. This is one purpose of fragilities, namely that they are developed independently from the hazard or occurrence rate essentially making them general and applicable to different sites. Structural damage from tsunamis is caused by water-borne debris and by direct hydrostatic, and in particular hydrodynamic forces. Approximate tsunami wave loading can be computed using a set of approximations proposed in FEMA P646 (2008). This approach provides an equivalent force expressed as a function of tsunami inundation height. Experimental and numerical studies (e.g. Neelamani et al. 1999; FEMA-P646 2008; Wilson et al. 2009) or incident wave conditions (Ramsden 1996) demonstrate that wave forces exerted on a structure are directly related to the wave height as one might expect. Despite continued scientific research, it remains very difficult to investigate the actual wave force, i.e. the actual wave pressure distribution, when the wave hits the structure mainly due to the combined water and air makeup of the tsunami bore.

Tsunami collapse fragilities are computed to show the conditional probability under tsunami loading with and without considering the influence of earthquakes, i.e. shaking. It is felt to be a logical extension from earthquake engineering to also apply fragility analysis to tsunami wave

loading (e.g., Koshimura et al. 2009). In earthquake engineering, probabilistic relationships between earthquake ground motion intensity (e.g. spectral acceleration) and structural damage (or another parameter, e.g. collapse) are the most typical fragilities. Ellingwood et al (2004) and Rosowsky and Ellingwood (2002) developed a fragility analysis methodology for assessing the response of light-frame wood construction exposed to extreme windstorms and earthquakes. Li and Ellingwood (2006) developed probabilistic risk assessment methods to determine the performance and reliability of low-rise light-frame wood residential construction in the United States subjected to hurricane hazards. Park and van de Lindt (2009) developed a fragility formulation which provided a method to assess the seismic vulnerability of a structure using existing shake table test data. A performance-based wind engineering approach that built on the logic of the Ellingwood et al (2004) study and was based on fragility curves was proposed by van de Lindt and Dao (2009). The majority of the above studies have successively relied upon experimental data in order to provide an accurate approach to both hazard and resistance for earthquakes and wind fragility development. The ability to accurately characterize tsunami hazard is somewhat lacking due to the rarity of these natural phenomena and, as mentioned above, the exact loading is believed to vary significantly depending on numerous physical variables such as topography.

Mathematical Formulation

Earthquake Models

The ten-parameter CUREE hysteresis model is applied in this study. A force-deformation response of a wood sheathing-to-framing connector has highly nonlinear behavior under

monotonic and cyclic loading. Initially, as loading is increased, the connector deforms and its connection starts losing capacity due to the wood fibers being crushed by the connector gradually. Equation (1) in order to capture the crushing between the wood framing and sheathing along with yielding of the connector can be determined a force using the relationship between input displacement and others displacement parameters, i.e. the ultimate displacement and the failure displacement.

$$P = \begin{cases} \text{sign}(\delta) (P_0 + r_1 K_0 |\delta|) [1 - \exp(-K_0 |\delta| / P_0)], & : |\delta| \leq |\delta_u| \\ \text{sign}(\delta) P_u + r_2 K_0 [\delta - \text{sign}(\delta) \delta_u], & : |\delta_u| < |\delta| \leq |\delta_F| \\ 0, & : |\delta| > |\delta_F| \end{cases} \quad (1)$$

where, K_0 is initial stiffness, P_0 is the initial force, r_1 is secondary stiffness factor, r_2 is tertiary stiffness factor, δ_u is the ultimate displacement, and δ_F is failure displacement, defined as the displacement occurs when the connector fails.

If the loading is reversed, i.e. under cyclic loading, the connector behaves as a pinched hysteresis loop. During the reversed-cyclic loading, hysteretic behavior is idealized by using a predefined set of load-paths to describe loading, unloading, and reloading. Initially, the loading rules follow the monotonic backbone curve described above. Unloading rules can be defined as piecewise linear segments using two degrading stiffnesses, $r_3 K_0$ and $r_4 K_0$. During unloading, the connector loses partial contact with the surrounding wood due to permanent deformation caused by previous loading. Reloading after unloading exhibits a pinching stiffness K_p where the pinching force P_l corresponds to zero-displacement and the reversal load path follows the unloading stiffness. The stiffness and strength degradation are defined using Equation (2):

$$K_p = K_0 \left(\frac{P_0}{\beta K_0 \delta_{UN}} \right)^\alpha \quad (2)$$

where, K_0 is an initial stiffness, F_0 is an initial force, α and β is degree of stiffness degradation parameter, and δ_{UN} is a last unloading displacement.

Specifically, the structure is modeled as an equivalent single-degree of freedom (SDOF) by using this hysteretic model. Detailed explanations of the CUREE model can be found in Folz and Filiatrault (2001) for the interested reader.

Tsunami loading

FEMA P646 (2008) proposed eight different types of wave force, three of which are considered in this study: (1) hydrostatic forces, (2) hydrodynamic forces, and (3) impulsive forces. Hydrostatic forces act when standing or slowly moving water meets a structure. It can be computed as:

$$F_h = \frac{1}{2} \rho_s g B h^2 \quad (3)$$

where, ρ_s is the fluid density including sediment, $1200 \text{ kg/m}^3 = 2.33 \text{ slugs/ft}^3$, g is the gravitational acceleration, B is the width of the structure or structural component, $h = (R - z_w)$ is the maximum water height above the base of the wall at the structure location, R is the run-up elevation at the structure location, and z_w is ground elevation at the structure location. Figure 4 depicts the physical meanings of these terms.

Also, from FEMA P646 (2008), when water flows around a structure, the hydrodynamic force can be computed as:

$$F_d = \frac{1}{2} \rho_s C_d B (hu^2)_{max} \quad (4)$$

where, ρ_s is the fluid density including sediment, $1200 \text{ kg} / \text{m}^3 = 2.33 \text{ slugs} / \text{ft}^3$, C_d is the drag coefficient, B is the width of the structure in the plane normal to the direction of flow, h is flow depth, and u is flow velocity at the location of the structure. In addition, impulsive forces are caused by the leading edge of a surge of water impacting a structure. It is conservatively recommended in FEMA P646 that the impulsive forces be taken as 1.5 times the hydrodynamic force and can be computed as:

$$F_s = 1.5 F_d \quad (5)$$

Detailed explanations of these three forces can be found in FEMA P646 (2008) and are not included here for brevity. Thus, the tsunami wave forces used in this study can be computed as the summation of these three forces and expressed as:

$$TWF = F_h + F_d + F_s \quad (6)$$

where, TWF is the total tsunami wave force. It is important to note that this study focuses on load and effect, but it is recognized that the load model is simplified and should be updated as relevant data becomes available.

In stage two of the analysis procedure, a nonlinear static pushover analysis is performed using these computed tsunami wave loads based on the tsunami inundation height under investigation. The computed wave forces are converted into an equivalent force and then applied to the SDOF system at the top of the wall, which is computed using basic force equilibrium. Figure 5 shows

the schematic procedure for computing the equivalent tsunami wave force. If the computed tsunami wave loading exceeds the structural capacity, the structure is assumed to have collapsed.

Fragility curves

A fragility curve is a conditional distribution that gives the probability of exceeding a specified threshold, e.g. drift, damage, or collapse, as a function of one or more hazard intensity measures. For earthquake hazard, intensity can be expressed in terms of spectral acceleration at the buildings fundamental period; for tsunami hazard it can be expressed in terms of tsunami inundation height. In essence, a fragility defines the conditional probability of the demand (D) placed upon the structure exceeding its capacity (C) for a given level of ground motion or tsunami inundation height intensity (I), and can be expressed as:

$$F = P[D \geq C | I] \quad (7)$$

where, F represents a fragility under given conditions.

Fragility Examples

Two seismic intensity levels described in terms of spectral acceleration which are commonly used in design and analysis are the Design Basis Earthquake (DBE) and Maximum Credible Earthquake (MCE), representing 10% and 2% exceedance probabilities in 50 years, respectively. All 44 ground motions (the 22 pairs summarized in Table 1) were used in stage one of the analysis for 44 earthquake analyses at each intensity level. Then, using the “damaged” model, tsunami analysis was performed to check the collapse of the structure under given wave conditions and heights. Variation in the tsunami inundation heights was introduced by applying a

range of coefficients of variation (COV), i.e. the ratio of standard deviation to the mean. Thus, it is possible to generate a suite of tsunami inundation heights using the COV. The tsunami inundation heights were generated in 0.1 meter increments from 0.0 meters to 5.0 meters. Each of those was treated as the mean tsunami inundation height for that analysis and the COV used to introduce dispersion about the mean. A log-normal distribution was arbitrarily assumed for the tsunami inundation height since log-normal distributions have been used extensively to introduce dispersion for other natural hazards. The coefficient of variation (COV) for tsunami inundation heights was computed from the publically accessible data described in Baldock et al. (2009) as 0.136 and is included as one of the COV values in the present study. That 13.6% variation was observed in a laboratory environment at Oregon State University where the tsunami was generated at exactly the same height and the wave basin topography was nominally identical. Thus, neglecting variation in the wave maker itself, it was felt to be reasonable to assume that when randomness in nature is introduced the COV is larger, i.e. 13.6% is a lower bound.

Two different types of fragility curves were generated in this study. The first type was constructed using tsunami analysis without earthquake analysis being performed first. The second type is the successive earthquake and tsunami analysis in order to quantify the influence and better understand how this type of successive loading affects fragilities. In order to analyze the system, initially a nonlinear time history analysis was performed using the earthquake record suite as described above. The damage from a single earthquake was allowed to remain numerically by keeping the strength and stiffness degradation in the hysteresis model representing the lateral force resisting system(s) for the structure and the tsunami loading described earlier was applied in the form of a nonlinear pushover analysis. This provides a single

analysis point. This procedure was repeated for thousands of combinations of earthquake and tsunami. The seismic intensity was held constant and all 44 records scaled to that intensity level, but the inundation height for the tsunami was allowed to possess a prescribed level of uncertainty in the form of the aforementioned COV. This results in thousands of successive combinations from which statistics and the resulting fragility can be computed.

A two-story light-frame wood structure was selected as an illustrative example. Each component of the building was modeled using the CUREE hysteresis model (Folz and Filiatrault 2001). The building was one unit of a two-story townhouse and its total living area is approximately 167 m^2 (1800 ft^2), with an attached two-car garage. The height of the townhouse from the first floor slab to the roof eaves was 5.49 meter (18 feet) and its total weight was approximately 36.3 tons (80 kips). The exterior walls of the two story example structure were covered on the outside with 22.23 cm (7/8 inch) thick stucco over 11.12cm (7/16 inch) thick OSB sheathed shear walls and 12.7 cm (1/2 inch) thick gypsum wallboard (drywall) was on the inside. The floor plan for this example, shown in Figure 6, is from the NEESWood benchmark test (Christovasilis et al. 2007), but the capacity was based on a typical Pacific Northwest design.

Consider the City of Cannon Beach, Oregon in the Pacific Northwest of the United States. According to the United State Geological Survey (USGS 2011) the design basis earthquake (DBE) and maximum credible earthquake (MCE) for the City of Cannon Beach have seismic intensities of 0.89g and 1.34g spectral acceleration at 0.2sec, $\xi = 5\%$, respectively. Degradation effects, when the two hazards are combined, are investigated first. Figure 7 shows the effects, which is based on one ground motion from the suite of records. The dashed line represents the

resistance of the building not considering seismic excitation which will be unity (normalized). The solid line represents the successive earthquake and tsunami analysis results and shows the degradation for this particular earthquake. The normalized resistance capacity has the same values when seismic excitation is not considered but reduces gradually when earthquake and tsunami analysis are considered. Approximately, 30% of the resistance capacity is reduced when the structure is subjected to the DBE (0.84g) level ground motion and 32% when MCE level (1.34g) is considered. However, Figure 7 depicts this reduction in structure capacity for only one earthquake within the suite of earthquakes. Now consider another earthquake from the suite, whose results are shown in Figure 8. For this earthquake one can see that the DBE level earthquake reduces the capacity by 54% and numerically fails the structure at a seismic intensity level even less than the MCE level.

This procedure is repeated for each of the earthquakes in the suite and then a nonlinear static pushover analysis is performed using the degraded backbone curve to represent the tsunami loads. It should be noted that the randomness in the earthquake is represented by the suite of earthquakes. The randomness in the tsunami force is represented through application of the COV to the inundation height as discussed earlier. Figure 9 shows the results of six analyses. Specifically, the solid line represents the resulting collapse fragility when only the tsunami (no earthquake) is considered. From the fragility one can read that a 1.96 meter inundation will collapse the building 50% of the time, whereas a 1.69 meter inundation will collapse the building 50% of the time if subjected to the MCE level earthquake first. While this may seem a minimal difference at first inspection this is with the lower bound COV inundation height considered. One can also observe from Figure 9 that the lower portion of the fragility is the earthquake

sensitive section, i.e. at MCE level there is a 22% chance of the earthquake collapsing the building prior to the tsunami reaching shore according to the model, used herein. Although these inundation heights are not large by recent tsunami hazards, the methodology for successive earthquake-tsunami analysis is the focus of this paper and has applicability across a range of building materials.

Now, consider Figure 10 which shows the same plot but with a tsunami COV of 50% and in the Y-direction of the building. Initially, the resulting collapse fragility seems to be slightly different when only the tsunami (no earthquake) and the DBE level earthquake are considered. This can be explained in that the building has more shearwalls in the Y-direction, thus one can expect it to be stronger and able to survive the DBE level earthquake without major damage that would have lead to the strength degradation of structural components, i.e. shearwalls. But the width of the building in the Y-direction is wider than that of the other direction, thus it is more vulnerable to tsunami hazard (Y is parallel to the shoreline) because it will take significantly more wave force. If the building has a 50% chance of collapse, for example, one can read that a 1.61 meter, 1.58 meter, and 1.43 meter inundation for tsunami-only, DBE level, and MCE level case, respectively. There is only 0.03 meter difference between the tsunami case and the DBE level earthquake case meaning there is no effect. One can also observe from Figure 10 that the fragility shows only a 9% chance of the MCE level earthquake collapsing the building prior to the tsunami reaching shore.

From these basic results one can observe that the tsunami inundation heights required to collapse a light-frame wood building decreased when the seismic intensity of the proceeding earthquake increases. The difference is not as notable as one might anticipate, but the trend is evident. The

methodology presented herein could be used to statistically determine requirements for vertical evacuation structures located in regions where near-field tsunamis are a risk such as the U.S. Pacific Northwest.

Summary and Conclusion

The objective of this study was to develop collapse fragilities for earthquake and tsunami loading thereby providing a basic method to quantify the design requirements for vertical evacuation structures. The combinations of a suite of earthquakes and tsunamis of varying inundation heights were applied to develop the fragilities to ensure the loads were as accurate as possible for the type of structure. The development of collapse fragility curves for subsequent earthquake and tsunami load can provide information needed to assess the vulnerability of structures and to provide key information related to vertical evacuation structures in near-field regions. It is these near-field regions that are (1) prone to ground shaking and (2) have insufficient tsunami warning time for evacuation due to the proximity of the offshore fault. The illustrative example in this paper focused on residential buildings and thus the inundation heights were only 2 to 4 meters, but it is envisioned that the approach may be extended to other structure types that are modeled nonlinearly with strength degradation. Extension to full structures and structure groups with the inclusion of drawdown and/or debris impact is needed to more fully quantify the applicability of vertical evacuation structures.

Acknowledgements

The material presented in this paper is based upon work supported by the National Science Foundation under Grant No. CMMI-0830378 (NEES Research) and CMMI-0402490 (NEES Operations). Any opinions, findings, and conclusions or recommendations expressed in this material are those of the author(s) and do not necessarily reflect the views of the National Science Foundation.

REFERENCE

T.E. Baldock, D. Cox, T. Maddux, J. Killian, and L. Fayler (2009). "Kinematics of breaking tsunami wavefronts: A data set from large scale laboratory experiments." *Coastal Engineering* 56: 506-516.

Ioannis P. Christovasilis, Andre Filiatrault, and Assawin Wanitkorkul (2007). "Seismic Testing of a Full-Scale Two-Story Light-Frame Wood Building: NEESWood Benchmark Test." Development of a performance-based seismic design philosophy for mid-rise woodframe construction, The State University of New York at Buffalo. Report NW-01.

Collins, M. S. (2009). "Finite Element Modeling of Light Frame Wood Structures an Integrated Approach." Civil Engineering. Raleigh, North Carolina, North Carolina State University. Doctor of Philosophy.

Bruce R. Ellingwood, David V. Rosowsky, Yue Li, and Jun Hee Kim (2004). "Fragility assessment of light-frame wood construction subjected to wind and earthquake hazards." *Journal of Structural Engineering* 130(12): 1921-1930.

FEMA-P646 (2008). "Guidelines for Design of Structures for Vertical Evacuation from Tsunamis." Washington, D.C., Federal Emergency Management Agency.

Folz, B. and A. Filiatrault (2001). "Cyclic Analysis of Wood Shear Walls." *Journal of Structural Engineering* 127(4): 433-441.

Folz, B. and A. Filiatrault (2004a). "Seismic analysis of woodframe structures. I: Model formulation." *Journal of Structural Engineering* 130(9): 1353-1360.

Folz, B. and A. Filiatrault (2004b). "Seismic analysis of woodframe structures. II: Model implementation and verification." *Journal of Structural Engineering* 130(9): 1361-1370.

Shunichi Koshimura, Takayuki OIE, Hideaki Yanagisawa, and Fumihiko Imamura (2009). "Developing fragility functions for tsunami damage estimation using numerical model and post-tsunami data from banda aceh, Indonesia." *Coastal Engineering Journal* 51(3): 243-273.

Li, Y. and B. R. Ellingwood (2006). "Hurricane damage to residential construction in the US: importance of uncertainty modeling in risk assessment." *Engineering Structures* 28: 1009-1018.

S. Neelamani, H. Schuttrumpf, M. Muttray, and H. Oumeraci (1999). "Prediction of wave pressures on smooth impermeable seawalls." *Ocean Engineering* 26: 739-765.

Park, S. and J. W. van de Lindt (2009). "Formulation of Seismic Fragilities for a Wood-Frame Building Based on Visually Determined Damage Indexes." *Journal of Performance of Constructed Facilities* 23(5): 346-352.

Shiling Pei and John W. van de Lindt (2008). "Manual of SAPWood for windows version 1.0." , Colorado State University, Fort Collins, CO.

Ramsden, J. D. (1996). "Forces on a vertical wall due to long waves, bores, and dry-bed surges." *Journal of Waterway, Port, Coastal, and Ocean Engineering* 122(3): 134-141.

Rosowsky, D. V. and B. R. Ellingwood (2002). "Performance-based engineering of wood frame housing: Fragility analysis methodology." *Journal of Structural Engineering* 128(1): 32-38.

USGS (2011). "U.S. Seismic Design Map ". Retrieved March, 2011, from <https://geohazards.usgs.gov/secure/designmaps/us/>.

van de Lindt, J. W. and T. N. Dao (2009). "Performance-Based Wind Engineering for Woodframe Buildings." *Journal of Structural Engineering* 135(2): 169-177.

Jebediah S. Wilson, Rakesh Gupta, John W. van de Lindt, Milo Clauson, and Rachel Garcia (2009). "Behavior of a One-Sixth Scale Wood-Framed Residential Structure under Wave Loading." *Journal of Performance of Constructed Facilities* 23(5): 336-345.

Xu, J. and J. D. Dolan (2009a). "Development of a Wood-Frame Shear Wall Model in ABAQUS." *Journal of Structural Engineering* 135(8): 977-984.

Xu, J. and J. D. Dolan (2009b). "Development of Nailed Wood Joint Element in ABAQUS." *Journal of Structural Engineering* 135(8): 968-976.

List of Tables

Table 1: Summary of ATC-63' 22 ground motions

ID No.	Earthquake			PGA Max(g)	
	M	Year	Name	Component1	Component2
1	6.7	1994	Northridge	0.42	0.52
2	6.7	1994	Northridge	0.41	0.48
3	7.1	1999	Duzce, Turkey	0.73	0.82
4	7.1	1999	Hector Mine	0.27	0.34
5	6.5	1979	Imperial Valley	0.24	0.35
6	6.5	1979	Imperial Valley	0.36	0.38
7	6.9	1995	Kobe, Japan	0.51	0.50
8	6.9	1995	Kobe, Japan	0.24	0.21
9	7.5	1999	Kocaeli, Turkey	0.31	0.36
10	7.5	1999	Kocaeli, Turkey	0.22	0.15
11	7.3	1992	Landers	0.24	0.15
12	7.3	1992	Landers	0.28	0.42
13	6.9	1989	Loma Prieta	0.53	0.44
14	6.9	1989	Loma Prieta	0.56	0.37
15	7.4	1990	Manjil, Iran	0.51	0.50
16	6.5	1987	Superstition Hills	0.36	0.26
17	6.5	1987	Superstition Hills	0.45	0.30
18	7.0	1992	Cape Mendocino	0.39	0.55
19	7.6	1999	Chi-Chi Taiwan	0.35	0.44
20	7.6	1999	Chi-Chi Taiwan	0.47	0.51
21	6.6	1971	San Fernando	0.21	0.17
22	6.5	1976	Friuli, Italy	0.35	0.31

Table 1: Summary of ATC-63's 22 ground motions (excerpted from FEMA P695 2009)

List of Figures

Figure 1: Remaining rubble in Talcahuano, Chile following a tsunami in 2010 (Photo Credit: John W. van de Lindt, University of Alabama)

Figure 2: Schematic overview of the two-stage analysis procedure used in this study

Figure 3: Example of a typical hysteretic model for illustrative purposes in this study

Figure 4: Details of tsunami inundation height parameter

Figure 5: Schematic procedure of computing equivalent tsunami wave force

Figure 6: Floor plan of test building (Christovasilis et al. 2007)

Figure 7: Degradation effects without any shearwalls failure case

Figure 8: Degradation effects with shearwalls failure case

Figure 9: Collapse probability of 13.6% COV when wave coming narrow width(X direction) of two-story building

Figure 10: Collapse probability of 50.0% COV when wave coming wide width(Y direction) of two-story building



FIG 1: Remaining rubble in Talcahuano, Chile following a tsunami in 2010 (Photo Credit: John W. van de Lindt, University of Alabama).

Sequential Seismic and Tsunami Analysis Program: SSTAP

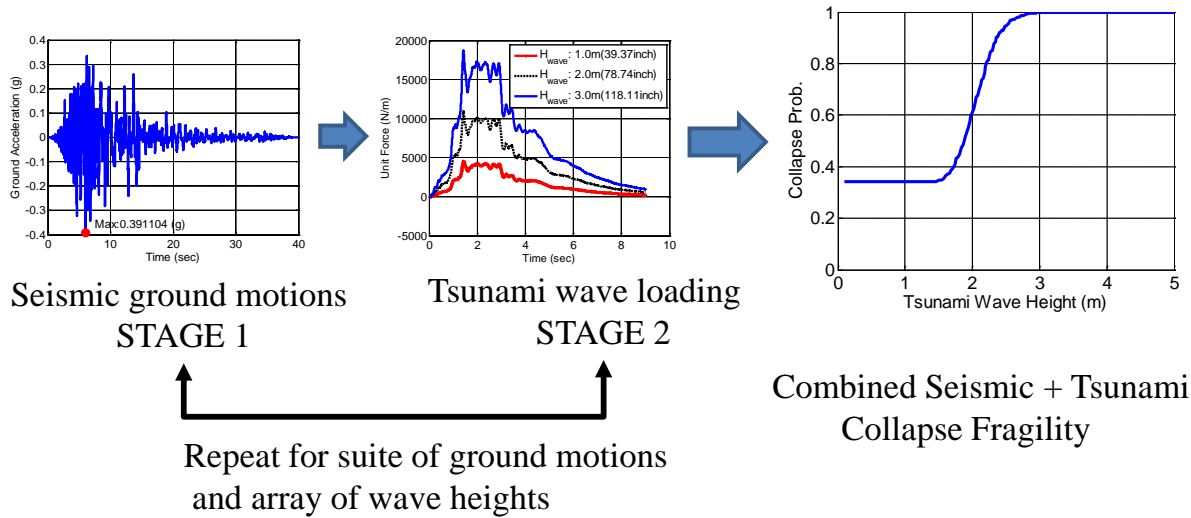


FIG 2: Schematic overview of the two-stage analysis procedure used in this study.

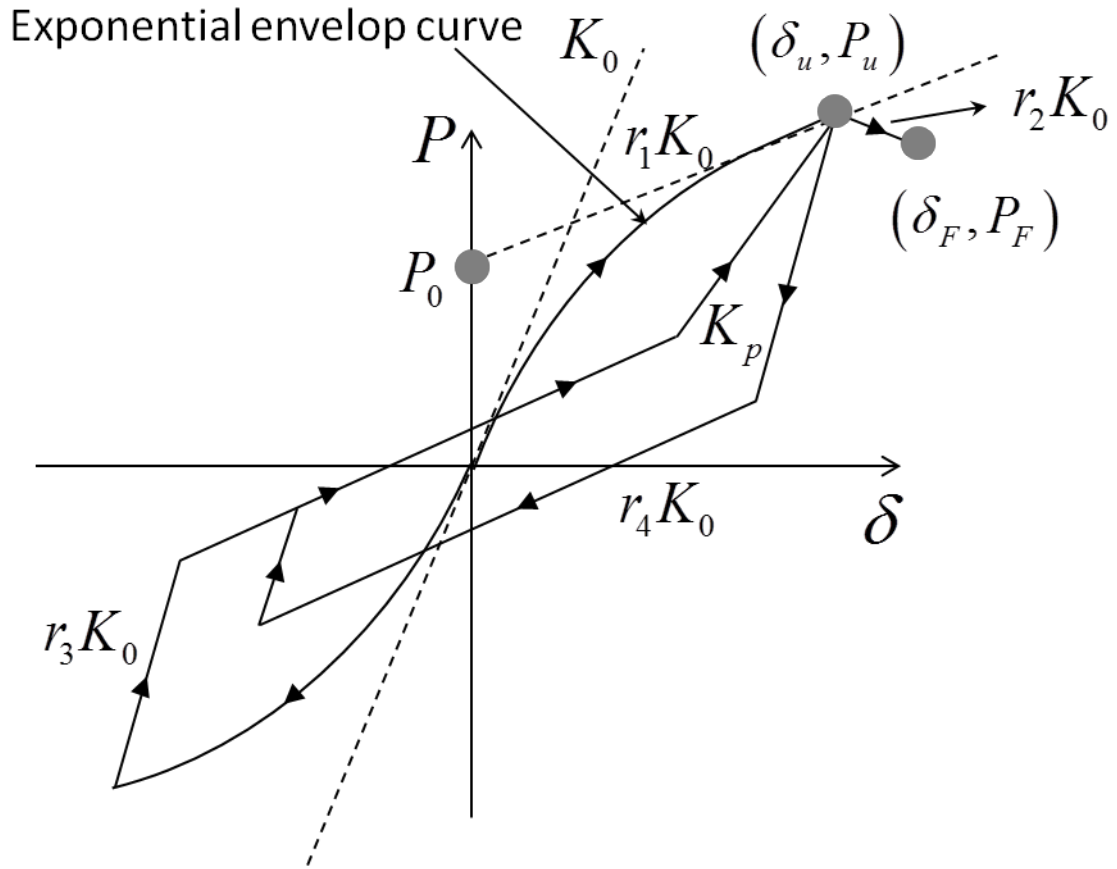


FIG 3: Example of a typical hysteretic model for illustrative purposes in this study.

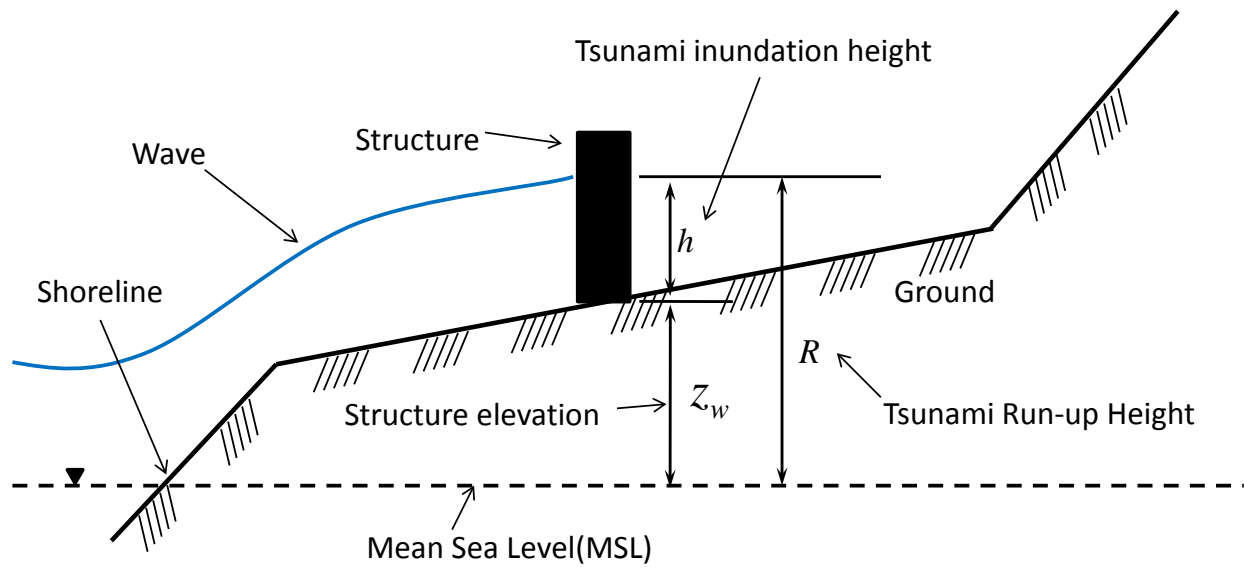


FIG 4: Details of tsunami inundation height parameter

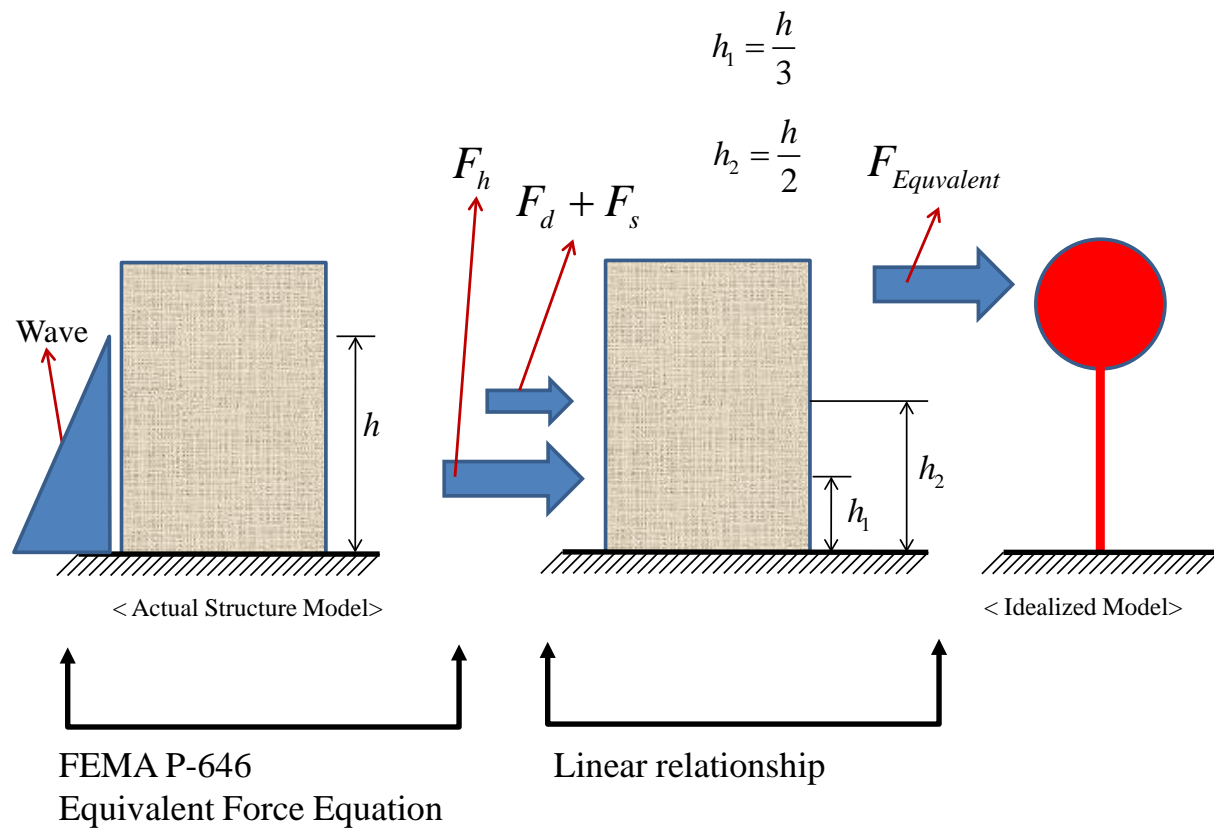


FIG 5: Schematic procedure of computing equivalent tsunami wave force

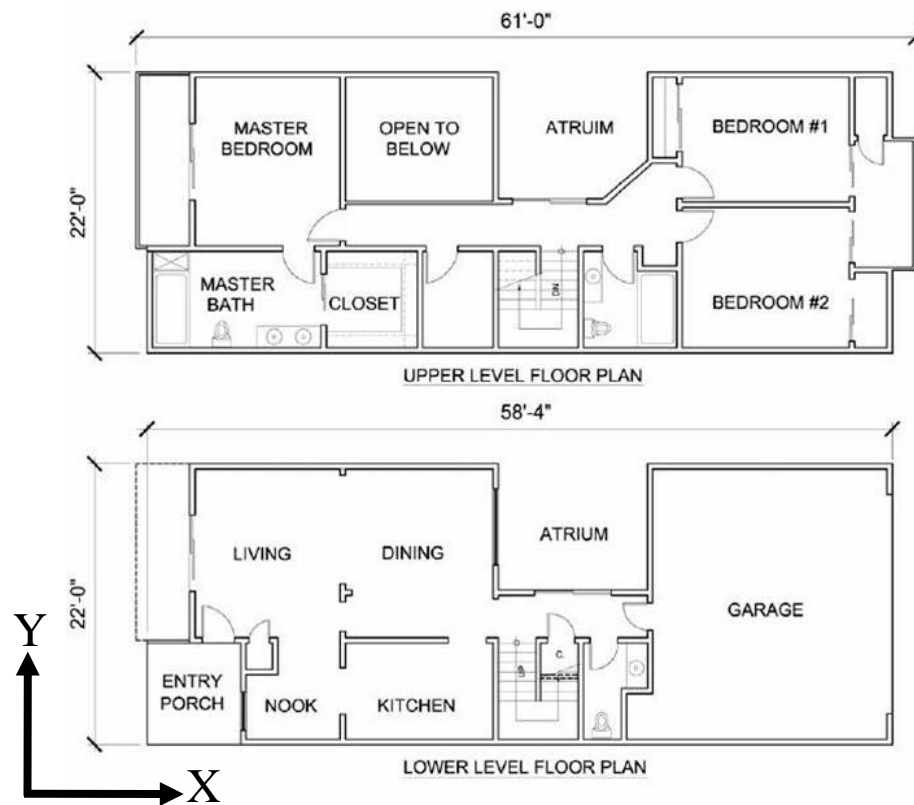


FIG 6 : Floor plan of test building (Christovasilis et al. 2007)

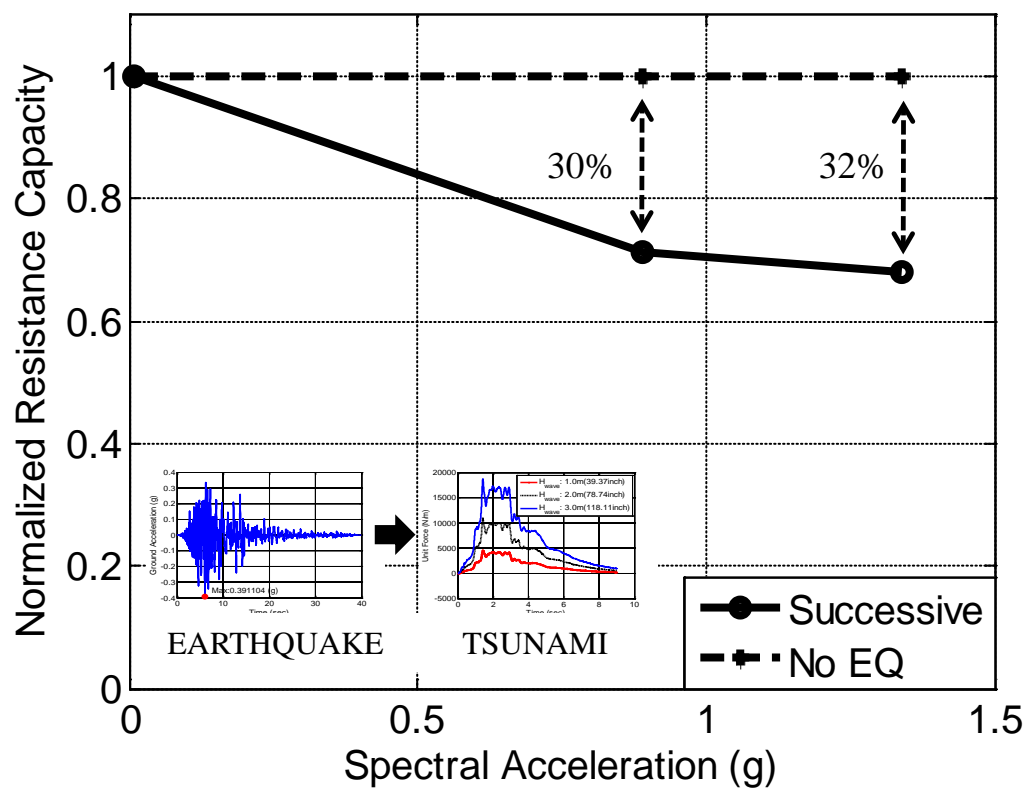


FIG 7: Degradation effects without any shearwalls failure case

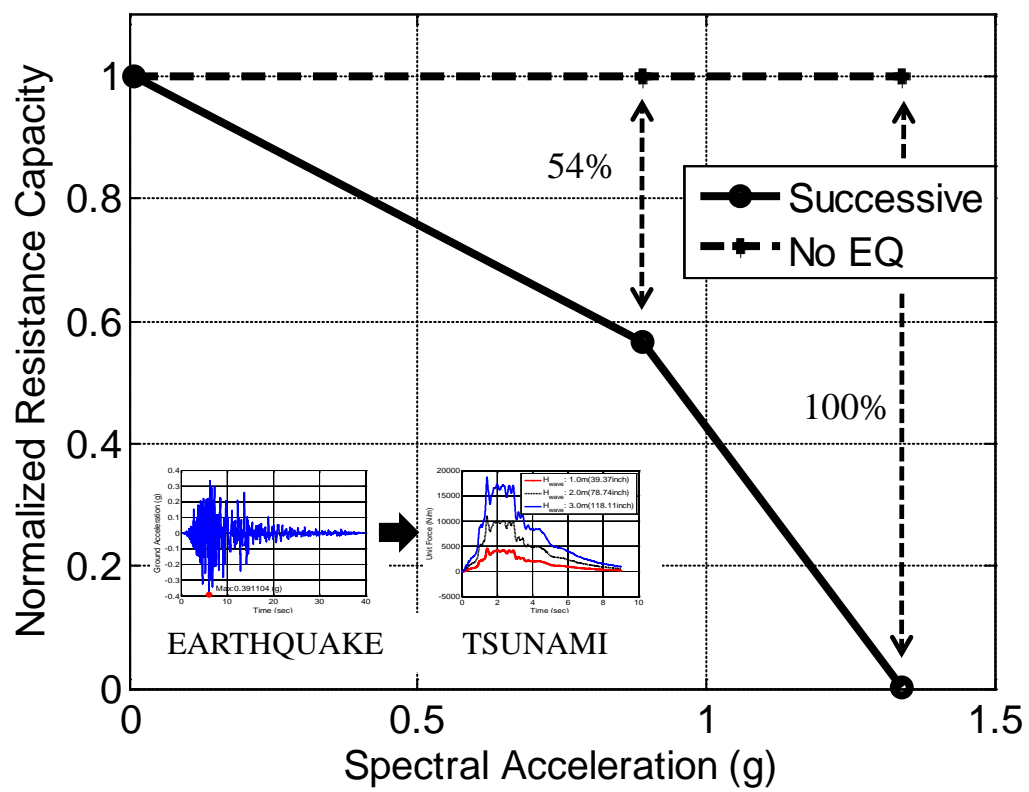


FIG 8: Degradation effects with shearwalls failure case

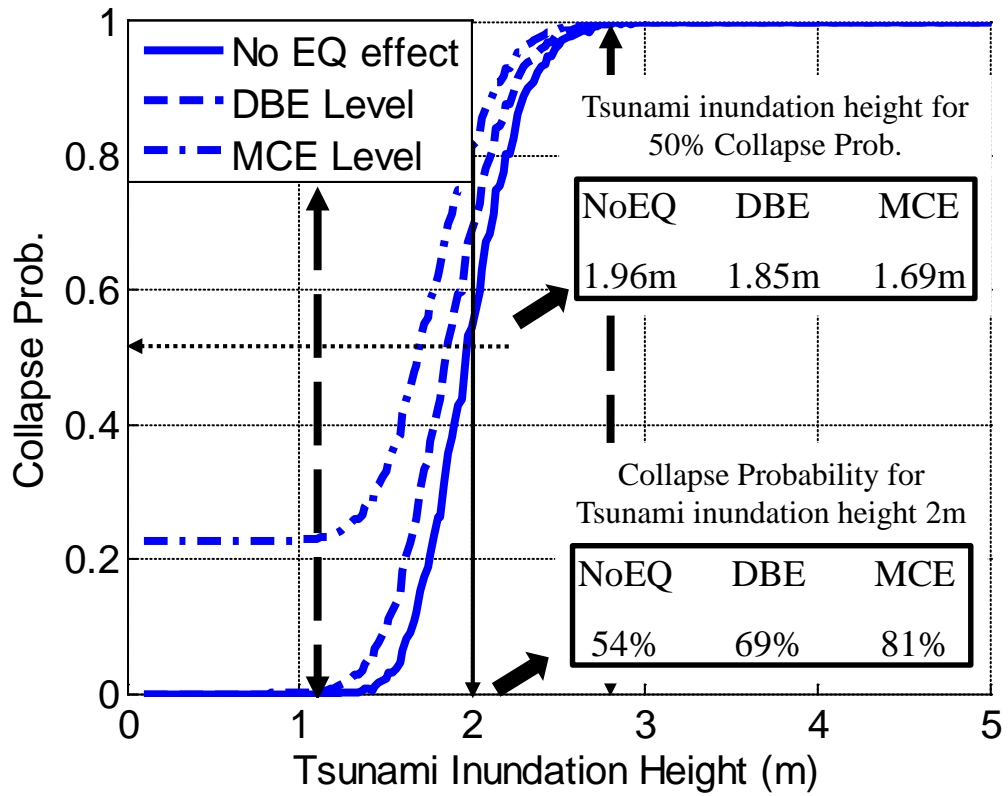


FIG 9: Collapse probability of 13.6% COV when wave coming narrow width(X direction) of two-story building

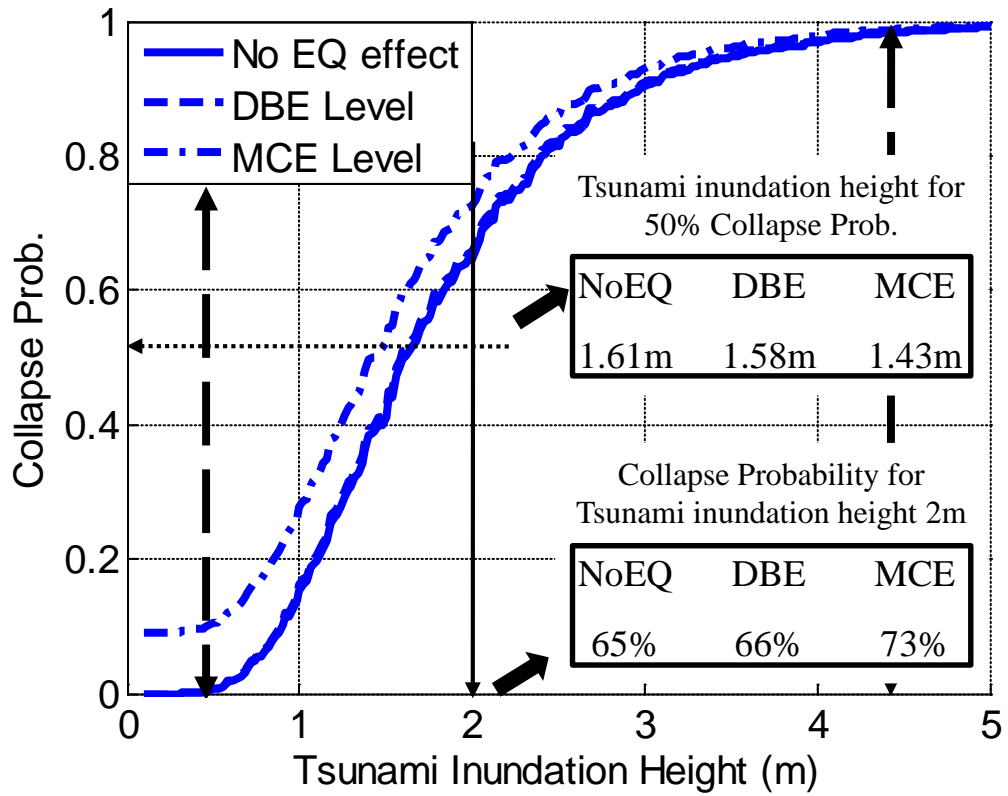


FIG 10: Collapse probability of 50.0% COV when wave coming wide width(Y direction) of two-story building